Higher-order linearly implicit one-step methods for three-dimensional incompressible Navier-Stokes equations

Ioan Teleaga, Jens Lang
Numerical Analysis and Scientific Computing
Darmstadt University of Technology
Department of Mathematics
Schlossgartenstr. 7
64289 Darmstadt
Germany

19.03.2007

Abstract

In this work higher-order methods for integrating the three-dimensional incompressible Navier-Stokes equations are proposed. The numerical solution is achieved by using linearly implicit one-step methods up to third order in time coupled with up to third order stable finite element discretizations in space. These orders of convergence are demonstrated by comparing the numerical solution with exact Navier-Stokes solutions. Finally, we present benchmark computations for flow around a cylinder.

Keywords: Navier-Stokes equations, Rosenbrock methods, finite element methods
2000 Mathematics Subject Classification: 76D05, 76M10

1 Introduction

Laminar incompressible flows play an important role in natural and industrial processes. For this type of flows the governing equations are the well known Navier-Stokes equations. Let $[0,T]\times\Omega$, $\Omega \subset \mathbb{R}^3$, be the computational domain, then the incompressible Navier-Stokes equations for viscous flows are

$$\begin{aligned} \partial_t U + (U\cdot\nabla)U + \nabla P - \nabla\cdot(2\nu\, S(U)) &= f, && \text{in } (0,T]\times\Omega \\ \nabla\cdot U &= 0, && \text{in } (0,T]\times\Omega \\ U &= U_b, && \text{on } (0,T]\times\partial\Omega \\ U &= U_0, && \text{in } \{0\}\times\Omega \\ \textstyle\int_\Omega P\,dx &= 0, && \text{in } [0,T] \end{aligned} \tag{1}$$

where ν is the viscosity of the fluid, and $U=(u,v,w)^T$, P, $S=(\nabla U+\nabla U^T)/2$ represent the velocity field, the pressure, and the stress tensor. The initial data U_0 and boundary data U_b have to be chosen such that system (1) describes a well posed problem.

Over the last years, there has been considerable development of numerical methods for solving numerically this set of equations [1]. The challenge nowadays consists in combining accuracy of the numerical solution and efficiency of the whole numerical algorithm.

This report extends the numerical methods based on linearly implicit one-step methods coupled with stabilized finite element discretizations in space presented in [6, 7] to three-dimensional incompressible Navier-Stokes equations. All of these methods are implemented in the finite element code KARDOS [5]. For this paper we will select two time integrators ROS2 and ROS3PL already included in the above mentioned code. ROS2 is an L-stable Rosenbrock solver of order 2 which is second order consistent for any approximation of the Jacobian matrix, and ROS3PL is an L-stable stiffly accurate Rosenbrock solver of order 3 which has no order reduction for PDEs with complex boundary conditions. It improves ROS3P [9] which is only A-stable. For a comparison of time-discretization and linearization approaches for the two-dimensional incompressible Navier-Stokes equations we refer to [4].

The basic solution algorithm contained in the KARDOS code also serves as a good foundation for developing new codes with other capabilities. For example, a scalar transport equation for the density can be easily added to investigate buoyancy driven flows. Additionally, these approaches can be improved using adaptive strategies based on a posteriori error estimates.

An outline of this paper is as follows. In Section 2 we recall the general discretization of the incompressible Navier-Stokes equations (1) according to our setting. Section 3 contains convergence studies and numerical results for a benchmark flow around a cylinder [11]. Finally, conclusions are presented in Section 4.

2 Discretization of the equations

Firstly, system (1) is discretized in time employing linearly implicit one-step methods to achieve higher-order temporal discretizations by working the Jacobian matrix directly into the integration formula [10, 2].

Let τ_n be a variable time step. Then an s-stage linearly implicit time integrator of Rosenbrock type applied to (1) reads as follows:

$$\begin{aligned} \tfrac{U_{ni}}{\gamma\tau_n} + (U_n\cdot\nabla)U_{ni} &+ (U_{ni}\cdot\nabla)U_n - \nabla\cdot(2\nu S(U_{ni})) + \nabla P_{ni} \\ &= f(t_i) - (U_i\cdot\nabla)U_i + \nabla\cdot(2\nu S(U_i)) - \nabla P_i \\ &\quad - \textstyle\sum_{j=1}^{i-1}\frac{c_{ij}}{\tau_n}U_{nj} + \tau_n\gamma_i\partial_t f(t_i), \\ -\nabla\cdot U_{ni} &= \nabla\cdot U_i, \end{aligned} \tag{2}$$

with $i = 1, ..., s$ and the internal values are given by

$$t_i = t_n + \alpha_i\tau_n, \quad U_i = U_n + \sum_{j=1}^{i-1} a_{ij}U_{nj}, \quad P_i = P_n + \sum_{j=1}^{i-1} a_{ij}P_{nj}.$$

The new solution (U_{n+1},P_{n+1}) at time $t_{n+1} = t_n + \tau_n$ is computed by

$$U_{n+1} = U_n + \sum_{j=1}^{s} m_j U_{nj}, \quad P_{n+1} = P_n + \sum_{j=1}^{s} m_j P_{nj}, \tag{3}$$

where the coefficients a_{ij}, c_{ij}, γ_i, α_i, and m_j are chosen such that they satisfy certain consistency conditions.

To estimate the error in time we make use of an embedding strategy. By replacing the coefficients m_j in (3) with different coefficients $\hat{m}_j$, a new solution $(\hat{U}_{n+1}, \hat{P}_{n+1})$ of inferior order, that is, order 1 for ROS2 and order 2 for ROS3PL. The difference

$$\delta_{n+1} \;:=\; ||(U_{n+1}, P_{n+1}) - (\hat{U}_{n+1}, \hat{P}_{n+1})||,$$

can be used as a step size control. A new step size with respect to a desired user tolerance TOL_t is selected by

$$\tau_{n+1} \;=\; C\frac{\tau_n}{\tau_{n-1}}\left(\frac{\delta_n\, TOL_t}{\delta_{n+1}\,\delta_{n+1}}\right)^{1/p}\tau_n, \tag{4}$$

where C represents a safety factor and is set to 0.95, and p denotes the order of the method used. Further details are given in [6, 8].

We describe now the derivation of the discrete equations obtained by a finite element discretization. Let $\mathcal{T}_h$ be an unstructured finite element mesh where the elements are tetrahedra, and S_h^q be the associated finite dimensional space with $q = 1, 2$ consisting of all continuous functions which are polynomials of order q on each tetrahedron $T \in \mathcal{T}_h$. In this way, the finite element approximation $U_{ni}^h \in S_h^q$ of the intermediate values U_{ni} in (2) has to satisfy the following equations

$$\begin{aligned}\left(\frac{U_{ni}^h}{\gamma\tau_n},\varphi\right) + \left((U_n^h\cdot\nabla)U_{ni}^h,\varphi\right) + \left((U_{ni}^h\cdot\nabla)U_n^h,\varphi\right) + \left(\nabla P_{ni}^h,\varphi\right) - \left(\nabla\cdot\left(2\nu S(U_{ni}^h)\right),\varphi\right)&\\ = \left(F^h(t_i,U_i^h,P_i^h),\varphi\right),&\\ -(\nabla\cdot U_{ni}^h,\varphi) = (\nabla\cdot U_i^h,\varphi),\ \forall\varphi\in S_h^q,\ i=1,...,s,&\end{aligned} \tag{5}$$

where $F^h(t_i, U_i^h, P_i^h)$ is the right hand side of the first equation in (2).

Equal-order finite element functions for all unknown components are used. However, in this case the Babuska-Brezzi conditions is not satisfied, resulting in spurious pressure modes in the discrete solution. A way to get a stable discretization is to relax the incompressibility constraint in (5) as follows

$$\begin{aligned}&-\left(\delta^h\,\nabla\cdot\left(\frac{U_{ni}^h}{\gamma\tau_n} + (U_n^h\cdot\nabla)U_{ni}^h + (U_{ni}^h\cdot\nabla)U_n^h - \nabla\cdot\left(2\nu S(U_{ni}^h)\right) + \nabla P_{ni}^h\right),\varphi\right)\\ &-\left(\nabla\cdot U_{ni}^h,\varphi\right) = \left(\nabla\cdot U_i^h,\varphi\right) - (\nabla\cdot F^h(t_i,U_i^h,P_i^h),\varphi),\ \forall\varphi\in S_h^q,\ i=1,...,s,\end{aligned}$$

with

$$\delta^h \;=\; c\,\frac{h_e}{2|u_e|}\frac{Re_e}{\sqrt{1+Re_e^2}},\quad Re_e = \frac{\rho_0 h_e u_e}{\nu},\quad c = 0.4,$$

where u_e and h_e are a global reference velocity and the diameter of the n-dimensional ball which is area-equivalent to an element $T \in \mathcal{T}_h$, respectively. Although, the incompressibility equation looks now rather complicated, to the version in (5) just the divergence of the discrete equation (2) times a local factor δ^h has been added.

For each unknown pair (U_{ni}^h, P_{ni}^h), $i = 1, .., s$, a linear system with one and the same stiffness matrix has to be solved. Then, the new solution is updated using (3). ROS2 requires two internal

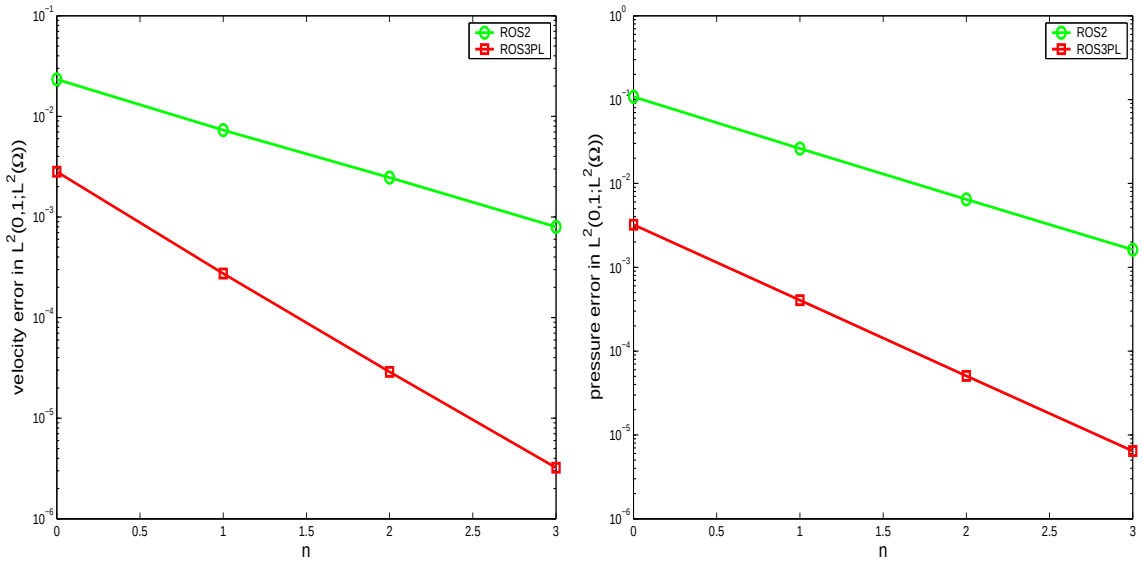

Figure 1: Time errors for ROS2 and ROS3PL, where n corresponds to $\tau = 0.5 \times 2^{-n}$.

stages for each time step, while ROS3PL requires four stages. Rosenbrock methods offer several structural advantages. From an efficiency point of view, the most important advantage is that no nonlinear systems have to be solved (which can be sometimes cumbersome). Moreover, there is no problem to construct Rosenbrock methods with optimum linear stability properties and no order reduction for stiff equations. Because of their one-step nature, they are easy to implement.

3 Numerical Results

In this section we first present convergence studies of our numerical methods using academic three-dimensional test problems with known solutions. Two examples address the temporal and spatial convergence properties of the proposed numerical methods. It will be shown that ROS2 and ROS3PL have second and third order accuracy in time, respectively. Next, convergence rates for spatial discretizations are presented. The last example shows results for the benchmark flow around a cylinder defined in [11].

3.1 An example to test the time discretization error

The first example allows us to check the order of the time discretization. On the integration domain $[0, T] \times \Omega$, $T = 1$, and $\Omega = (0, 1)^3$, we consider (1) with the exact solution

$$\begin{aligned} u &= y^2 \exp(-t), \\ v &= z^2 \exp(-t), \\ w &= x^2 \exp(-t), \\ p &= (x + y + z) \exp(-t). \end{aligned}$$

The right-hand side f, the initial condition U_0 and the boundary condition U_b are chosen accordingly. The viscosity is set to 10^{-3}. The simulations are performed with quadratic elements

on a fixed uniform mesh with 70400 tetrahedra. In this way, for any time t the temporal error will dominate the spatial error. The computations were done for fixed time steps $\tau = 0.5 \times 2^{-n}$, $n = 0, 1, 2, 3$.
We study the velocity and pressure errors in the norm $L^2(0,1;L^2(\Omega))$, i.e.,

$$||U - U^h||_{L^2(0,1;L^2(\Omega))} = \left(\int_0^1 ||(U - U^h)(t)||^2_{L^2(\Omega)} dt \right)^{1/2},$$
$$||P - P^h||_{L^2(0,1;L^2(\Omega))} = \left(\int_0^1 ||(P - P^h)(t)||^2_{L^2(\Omega)} dt \right)^{1/2}.$$

Figure 1 presents convergence results for both velocity (left) and pressure (right) components. ROS2 shows second order accuracy, while ROS3PL shows third order accuracy in all components. The best velocity and pressure error in $L^2(0,1;L^2(\Omega))$ has been obtained by the ROS3PL scheme. ROS2 induces for large time steps larger errors in both velocity and pressure components. For long time computations ROS3PL is more efficient with respect to CPU time.

3.2 An example to test the spatial discretization error

The following exact three-dimensional test solution to the incompressible Navier-Stokes equations has been proposed in [13]:

$$\begin{aligned} u &= \sin(mx)\cos(ly)\cos(nz)\exp(-t\nu), \\ v &= -\frac{m+n}{l}\cos(mx)\sin(ly)\cos(nz)\exp(-t\nu), \\ w &= \cos(mx)\cos(ly)\sin(nz)\exp(-t\nu), \end{aligned} \tag{6}$$

where m, n, l define the wave numbers along all three directions. The pressure is determined by assuming no force in the y- direction, that is,

$$\begin{aligned} p &= -\frac{(m+n)\nu}{l^2}\cos(mx)\cos(ly)\cos(nz)\exp(-t\nu) \\ &\quad + \frac{m(m+n)}{4l^2}\sin^2(mx)\cos(2ly)\cos^2(nz)\exp(-2t\nu) \\ &\quad + \frac{(m+n)^2}{4l^2}\cos^2(mx)\cos(2ly)\cos^2(nz)\exp(-2t\nu) \\ &\quad + \frac{m(m+n)}{4l^2}\cos^2(mx)\cos(2ly)\sin^2(nz)\exp(-2t\nu). \end{aligned} \tag{7}$$

The other forces are determined such that (6)-(7) form an exact solution to the Navier-Stokes equations. For the sake of simplicity, the computational domain is the unit cube, and we set $m = n = l = 1$, and viscosity $\nu = 1$. To test the convergence error in space with linear elements we apply the ROS2 time solver. The results for this combination are presented in Table 1. As expected, this numerical scheme preserves second-order accuracy in space at the final time $T = 1$.

The simulation was done with a fixed time step $\tau = 10^{-2}$. Indeed, time errors induced by ROS2 were settled down. For the test with quadratic elements we have chosen ROS3PL time solver. Table 2 shows results for this numerical scheme.

Grid level		L^2-norm (OOC)	Max-norm (OOC)
$h = 1/4$	u	3.38e-03	7.47e-03
	v	5.78e-03	1.52e-02
	w	2.78e-03	7.61e-03
$h = 1/8$	u	8.35e-04 (2.01)	2.05e-03 (1.86)
	v	1.44e-03 (2.00)	4.06e-03 (1.90)
	w	7.13e-04 (1.96)	1.99e-03 (1.93)
$h = 1/16$	u	2.06e-04 (2.01)	5.58e-04 (1.87)
	v	3.57e-04 (2.01)	1.08e-03 (1.91)
	w	1.78e-04 (1.99)	5.54e-04 (1.84)

Table 1. Error-norms and numerically observed order of convergence (OOC) for ROS2 with linear elements at time $T = 1$.

Grid level		L^2-norm (OOC)	Max-norm (OOC)
$h = 1/4$	u	5.85e-05	2.77e-04
	v	1.22e-04	5.42e-04
	w	6.28e-05	3.09e-04
$h = 1/8$	u	7.76e-06 (2.91)	3.96e-05 (2.80)
	v	1.57e-05 (2.95)	7.95e-05 (2.76)
	w	8.18e-06 (2.94)	4.18e-05 (2.88)
$h = 1/16$	u	1.01e-06 (2.94)	5.37e-06 (2.88)
	v	2.04e-06 (2.94)	1.13e-05 (2.81)
	w	1.07e-06 (2.93)	5.52e-06 (2.92)

Table 2. Error-norms and numerically observed order of convergence (OOC) for ROS3PL with quadratic elements at $T = 1$.

The observed order of convergence in space is nearly three. Here the time step used was $\tau = 10^{-1}$. In engineering computations it is very important to have robust solvers which allow large time steps. In this sense ROS3PL behaves adequately and will be used in our further turbulence research.

3.3 Flow around a cylinder

This benchmark problem has been defined within the DFG high priority research program "Flow simulation with high-performance computers".

Figure 2 shows the considered computational domain where $L = 2.25$ m, $H = 0.41$ m, and the diameter of the cylinder is $D = 0.1$ m. The purpose of this benchmark is to numerically evaluate

- the drag force, i.e., $C_D = \int_S \left(\rho\nu \frac{\partial U_t}{\partial n} n_y - P n_x\right) dS$
- the lift force, i.e., $C_L = -\int_S \left(\rho\nu \frac{\partial U_t}{\partial n} n_x + P n_y\right) dS$
- the pressure difference $\Delta P(t) = P(0.45, 0.20, 0.205) - P(0.55, 0.20, 0.205)$

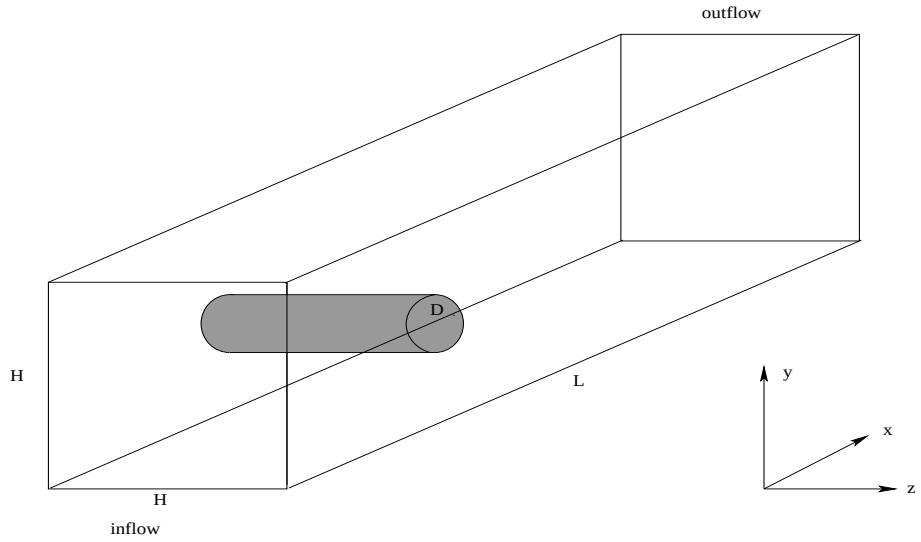

Figure 2: The computational geometry.

where S, $n = (n_x, n_y, 0)^T$, U_t, $t = (n_y, -n_x, 0)$ represent the cylinder surface, the normal vector on S, the tangential velocity on S, and the tangent vector respectively. Further, the viscosity of the fluid is $\nu = 0.001\ m^2/s$, and the density is $\rho = 1\ kg/m^3$. Then the drag and lift coefficients are defined to be

$$c_D = \frac{2C_D}{\rho \overline{u}^2 DH}, \quad c_L = \frac{2C_L}{\rho \overline{u}^2 DH},$$

where $\overline{u} = 4u(0, H/2, H/2, t)$ represents the characteristic velocity. Next, for our computations we take the following two benchmark cases from [11]:

- Case 1 (steady): The inflow boundary condition is

$$u(0, y, z) = 16u_m yz(H - y)(H - z)/H^4,\ v = w = 0$$

  with $u_m = 0.45m/s$. The corresponding Reynolds number is 20 based on u_m, D, and ν.

- Case 2 (unsteady): The inflow boundary condition is

$$u(0, y, z) = 16u_m yz(H - y)(H - z)sin(\pi t/8)/H^4,\ v = w = 0$$

  with $u_m = 2.25m/s$. The simulation time is $0 \leq t \leq 8\,s$. The corresponding Reynolds number is 100 based on u_m, D, and ν.

A complete description of these cases can be found in [11].
The mesh used for these tests consists of 14148 points and is presented in Figure 3. Using less grid points we were unable to obtain the drag and lift coefficient values even for the first test case. The discretization near the cylinder has a crucial importance. Two boundary layers around the cylinder have been used to ensure a proper resolution. The minimum grid spacing between the cylinder and the first layer was set to 0.005, while the grid spacing between the second layer and the cylinder was set to 0.01. Moreover, each cross-section of the cylinder in z- direction has

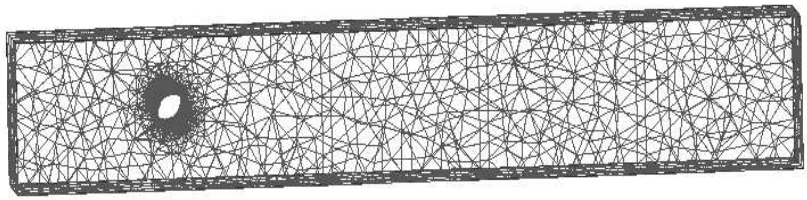

Figure 3: The mesh used

been resolved with 32 points. We will restrict ourselves to linear elements. A comparison of the drag and lift coefficients and pressure difference at steady state with benchmark results from [11] and [3] is shown in Table 3. Both ROS2 and ROS3PL time schemes produce good results.

	ROS2	ROS3PL	Ref. [3]	Benchmark [11]
c_D	6.1199	6.1199	6.1853	6.0500 - 6.2500
c_L	0.0195	0.0195	0.009400	0.0080 - 0.0100
Δp	0.1725	0.1725	0.1707	0.1650 - 0.1750

Table 3. Comparison of drag and lift coefficient and pressure difference for Case 1.

	ROS2	ROS3PL	Benchmark [11]
c_D	3.1617	3.1558	3.2000 - 3.3000
c_L	0.0120	0.0110	0.0020 - 0.0040
Δp	-0.1191	-0.1183	-0.0900 - -0.1100

Table 4. Comparison of drag and lift coefficient and pressure difference for Case 2.

In Table 4 we present results for the second test case. Here, using less grid points as the authors in [11] we obtain similar coefficients with small variations. For all these cases the simulation was run with adaptive time steps according to equation (4). Although the drag coefficient is relatively simple to obtain, the lift coefficient is very sensitive to the mesh near the cylinder. For more accurate results one need to construct meshes with a better resolution of the cylinder region.
The linear systems arising from every time-stage are solved with the BiCGStab algorithm [12] with ILU as a preconditioner.

4 Conclusions

In this paper we have presented numerical methods based on linearly implicit time schemes of Rosenbrock type and stabilized finite elements in space to numerically solve laminar flow problems described through the three-dimensional incompressible Navier-Stokes equations. All

these methods have been included in our adaptive finite element code KARDOS. The numerical examples studied in Section 3 clearly reveal second and third order of accuracy in space and time for our schemes. More specifically, applied to laminar flow problems with known smooth solutions, ROS2 and ROS3PL show their theoretical time order two and three, respectively. In these cases, ROS3PL performs more efficiently with respect to computing time. Our stabilization technique in space allows us to use equal-order finite elements for velocity and pressure components. We have found that combined with a Rosenbrock solver of suitable order, linear and quadratic Lagrange elements yield second and third order of spatial accuracy measured in the L^2- and maximum norm. From further practical experiences, our approach appears to provide a promising starting point for the development of efficient numerical solvers for more complex, turbulent flows. In our future work we are extending our code KARDOS to study and validate subgrid-scale models in the context of large eddy simulations for various physical applications.

Acknowledgement

This work has been supported by the German Research Foundation (DFG) through the Grant SFB-568 "Flow and Combustion in Future Gas Turbine Combustion Chambers" at the TU Darmstadt.

References

[1] R. Glowinski, *Finite element methods for incompressible viscous flow*, in Numerical Methods for fluids (Part 3), Ciarlet P.G., *et al.* (eds), Handbook of Numerical Analysis, Vol. IX, North-Holland, 2003.

[2] E. Hairer, G. Wanner, *Solving Ordinary Differential Equations II, Stiff and Differential-Algebraic Problems*, Second Revised Edition, Springer-Verlag, Berlin, Heidelberg, New York, 1996.

[3] V. John, *Higher order finite element methods and multigrid solvers in a benchmark problem for the 3D Navier-Stokes equations*, Int. J. Num. Meth. Fluids, **40**(2002), pp. 775 - 798.

[4] V. John, G. Matthies, J. Rang, *A comparison of time-discretization/linearization approaches for the time-dependent incompressible Navier-Stokes equations*, Comput. Meth. Appl. Mech. Engrg., **195**(2006), pp. 5995 - 6010.

[5] KARDOS, http://www.zib.de/Numerik/numsoft/kardos/

[6] J. Lang, *Adaptive Multilevel Solution of Nonlinear Parabolic PDE Systems. Theory, Algorithm and Applications*, Lectures Notes in Computational Science and Engineering, Vol. 16, Springer Verlag, 2000.

[7] J. Lang, *Adaptive Incompressible Flow Computations with Linearly Implicit Time Discretization and Stabilized Finite Elements*, in K.D. Papailiou, D. Tsahalis, J. Periaux, C. Hirsch, M. Pandolfi (eds.), Computational Fluid Dynamics 1998, John Wiley & Sons, New York, 1998, pp. 200-204.

[8] J. Lang, *Adaptive FEM of reaction-diffusion equations*, Appl. Numer. Math., **26**(1998), pp. 105-116.

[9] J. Lang, J. Verwer, *ROS3P - an Accurate Third-Order Rosenbrock Solver Designed for Parabolic Problems*, BIT, **41**(2001), pp. 730-737.

[10] H.H. Rosenbrock, *Some general implicit processes for the numerical solution of differential equations*, Computer J., **5**(1963), pp. 329-331.

[11] M. Schäfer, S. Turek, *Benchmark Computations of laminar flow around cylinder*, in Flow Simulation with High-Performance Computers II volume 52 of Notes on Numerical Fluid Mechanics, Braunschweig, Vieweg, 1996, pp 547-566,

[12] H.A. van der Vorst, *BI-CGSTAB: a fast and smoothly converging variant of BI-CG for the solution of nonsymmetric linear systems*, SIAM J. Sci. Statist. Comput., **13**(1992), pp. 631-644.

[13] J. Xu, D. Xiu, G.E. Karniadakis, *A Semi-Lagrangian method for turbulence simulations using mixed spectral discretizations*, J. Sci. Computing, **17**(2002), pp. 585-597.